
SHAPE OPTIMIZATION FOR THE MITIGATION OF COASTAL EROSION VIA SHALLOW WATER EQUATIONS

 **Luka Schlegel**

Department of Mathematics
Universität Trier
Universitätsring 15, 54296 Trier
schlegel@uni-trier.de

 **Volker Schulz**

Department of Mathematics
Universität Trier
Universitätsring 15, 54296 Trier
volker.schulz@uni-trier.de

September 16, 2022

ABSTRACT

Coastal erosion describes the displacement of land caused by destructive sea waves, currents or tides. Major efforts have been made to mitigate these effects using groins, breakwaters and various other structures. We address this problem by applying shape optimization techniques on the obstacles. We model the propagation of waves towards the coastline using two-dimensional shallow water equations with artificial viscosity. The obstacle's shape is optimized over an appropriate cost function to minimize the mechanical energy and to reduce velocities of water waves along the shore, without relying on a finite-dimensional design space, but based on shape calculus.

1 Introduction

Coastal erosion describes the displacement of land caused by destructive sea waves, currents and/or tides. Major efforts have been made to mitigate these effects using groins, breakwaters and various other structures. Among experimental set-ups to model the propagation of waves towards a shore and to find optimal wave-breaking obstacles, the focus has turned towards numerical simulations due to the continuously increasing computational performance. Essential contributions to the field of numerical coastal protection have been made for steady [1][2][3] and unsteady [4][5] descriptions of propagating waves. In this paper we select one of the most widely applied system of wave equations. We describe the hydrodynamics by the set of Saint-Venant or better known as shallow water equations (SWE), that originate from the famous Navier-Stokes equations by depth-integration, based on the assumption that horizontal length-scales are much larger than vertical ones [6]. Calculating optimal shapes for various problems is a vital field, combining several areas of research. This paper builds up on the monographs [7][8][9] to perform free-form shape optimization. In addition, we strongly orientate on [10][11][12] that use the Lagrangian approach for shape optimization, i.e. calculating state, adjoint and the deformation of the mesh via the volume form of the shape derivative assembled on the right-hand-side of the linear elasticity equation, as Riesz representative of the shape derivative. The calculation of the SWE continuous adjoint and shape derivative and its use in free-form shape optimization appears novel to us. However, we would like to emphasize, that the SWE have been used before in the optimization of practical applications, e.g. using discrete adjoints via automatic differentiation in the optimization of the location of tidal turbines [13] and to optimize the shape of fish passages in finite design spaces [14][15].

The paper is structured as follows: In Section 2 we formulate the PDE-constrained optimization problem. In Section 3 we derive the necessary tools to solve this problem, by deriving adjoint equations and the shape derivative in volume form. The final part, Section 4, will then apply the results to firstly a simplified mesh and secondly to more realistic meshes, picturing first the Langue de Barbarie (LdB), a coastal section in the north of Dakar, Senegal that was severely affected by coastal erosion within the last decades and secondly a global illustration in the form of a spherical world mesh.

2 Problem Formulation

Suppose we are given an open domain $\tilde{\Omega} \subset \mathbb{R}^2$, which is split into the disjoint sets $\Omega, D \subset \tilde{\Omega}$ such that $\Omega \cup D \cup \Gamma_3 = \tilde{\Omega}$, $\Gamma_1 \cup \Gamma_2 = \partial\tilde{\Omega}$. We assume the variable, interior boundary Γ_3 and the fixed outer $\partial\tilde{\Omega}$ to be at least Lipschitz. One simple example of such kind is visualized below in Figure 1.

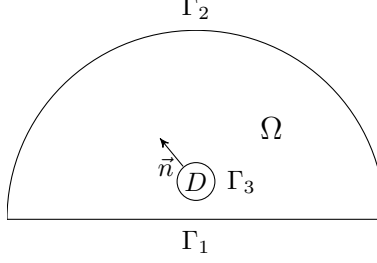


Figure 1: Illustrative Domain Ω with Initial Circled Obstacle D and Boundaries Γ_1, Γ_2 and Γ_3

On this domain we model water wave and velocity fields as solution to SWE with artificial viscosity, i.e.

$$\partial_t U + \nabla \cdot F(U) - \nabla \cdot (G(\mu) \nabla \hat{U}) = S(U) \quad \text{in } \Omega \times (0, T), \quad (1)$$

where we are given the SWE in vector notation with flux matrix

$$F(U) = \begin{pmatrix} \vec{Q} & \vec{Q} \\ \vec{Q} \otimes \vec{Q} + \frac{1}{2} g H^2 \mathbf{I}_2 & \end{pmatrix} = \begin{pmatrix} Hu & vH \\ Hu^2 + \frac{1}{2} g H^2 & Huv \\ Huv & Hv^2 + \frac{1}{2} g H^2 \end{pmatrix} \quad (2)$$

for identity matrix $\mathbf{I}_2 \in \mathbb{R}^{2 \times 2}$, gravitational acceleration g and solution $U : \Omega \times (0, T) \rightarrow \mathbb{R} \times \mathbb{R}^2$, where for simplicity the domain and time-dependent components are denoted by $U = (H, \vec{Q}) = (H, Hu, Hv)$, with H being the water height and Hu, Hv the weighted horizontal and vertical discharge or velocity. For notational ease, we set $\hat{U} = (H + z, \vec{Q})$ for scalar sediment height $z : \Omega \rightarrow \mathbb{R}$. The setting can be taken from Figure 2. The source term in (1)

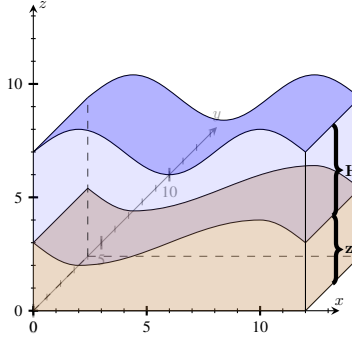


Figure 2: Cross-Section for Identification of Wave Height H and Sediment Height z

is defined as

$$S(U) = \begin{pmatrix} 0 \\ -gH \frac{\partial z}{\partial x} - gHu \frac{\sqrt{u^2 + v^2}}{KH^{4/3}} \\ -gH \frac{\partial z}{\partial y} - gHv \frac{\sqrt{u^2 + v^2}}{KH^{4/3}} \end{pmatrix}, \quad (3)$$

where the first term responds to variations in the bed slope and the second term is resembling the Manning formula to respond to bottom friction, where $K > 0$ is Manning's roughness coefficient [16, Section 3.3.2]. For the boundaries we use rigid-wall and outflow conditions for Γ_1, Γ_3 and Γ_2 by setting the velocity in normal direction to zero and prescribing a water height H_1 at the boundary, such that

$$\begin{aligned} \vec{Q} \cdot \vec{n} = 0, \nabla(H + z) \cdot \vec{n} = 0, \nabla Q_1 \cdot \vec{n} = 0, \nabla Q_2 \cdot \vec{n} = 0 & \quad \text{on } \Gamma_1, \Gamma_3 \times (0, T) \\ H = H_1, \nabla Q_1 \cdot \vec{n} = 0, \nabla Q_2 \cdot \vec{n} = 0 & \quad \text{on } \Gamma_2 \times (0, T). \end{aligned} \quad (4)$$

Initial conditions for U are implemented by prescribing a fixed starting point U_0 , i.e.

$$U = U_0 \quad \text{in} \quad \Omega \times \{0\} \quad (5)$$

Remark. Original viscous SWE are an incomplete parabolic system, where viscosity is only placed on the momentum equation. To prevent shocks or discontinuities that can appear in the original formulation of the hyperbolic SWE even for continuous data in finite time, an additional viscous term is added in the continuity equation such that we obtain a set of fully parabolic equations. We control the amount of added diffusion by the diagonal matrix $G(\mu) = \sum_{i=1}^n e_i^T \mu e_i e_i^T$ with entries $\mu = (\mu_v, \mu_f) \in \mathbb{R}_+ \times \mathbb{R}_+^2$ and basis vector $e_i \in \mathbb{R}^n$ with n being the number of dimensions in vector μ . In this setting μ_f is fixed, while we rely on shock detection in the determination of μ_v following [17]. Ultimately, a physical interpretation can be obtained for the introduction of the viscous part in the conservation of momentum equations. However, μ_v is solely based on stabilization arguments, where we follow the justification as in [18]. The complete parabolic problem together with well-posed boundary conditions [19] provides us with a well-posed problem.

We obtain a PDE-constrained optimization problem for objective

$$J(\Omega) = J_1(\Omega) + J_2(\Omega) + J_3(\Omega) + J_4(\Omega) + J_5(\Omega), \quad (6)$$

where we are trying to minimize the mechanical wave energy of destructive waves at the shore Γ_1 , that are waves above a critical threshold $H_{cr} > 0$ [2], over a time window $\tilde{T} \subset (0, T)$, i.e.

$$J_1(\Omega) = \int_{\tilde{T}} \int_{\Gamma_1} \nu_1 E \sigma_\alpha (H - H_{cr}) \, ds \, dt \quad (7)$$

for mechanical wave energy $E = \frac{1}{8} \rho g H^2$ and reduction to destructive sea waves enforced by usage of the sigmoid function $\sigma_\alpha : \mathbb{R} \rightarrow \mathbb{R}$ with slope parameter $\alpha > 0$. In addition, we aim for zeroed velocities

$$J_2(\Omega) = \int_0^T \int_{\Gamma_1} \frac{\nu_2}{2} \|\vec{Q}\|_2^2 \, ds \, dt. \quad (8)$$

These objectives are supplemented by a volume penalty and a perimeter regularization, i.e.

$$J_3(\Omega) = -\nu_3 \int_{\Omega} 1 \, dx, \quad (9)$$

and

$$J_4(\Omega) = \nu_4 \int_{\Gamma_3} 1 \, ds. \quad (10)$$

Additionally, a minimal thinness penalty on obstacle level is added by following [20] as

$$J_5(\Omega) = \nu_5 \int_{\Gamma_3} \int_0^{d_{min}} [(d_\Omega(x - \xi \vec{n}(x)))^+]^2 \, d\xi \, ds. \quad (11)$$

Here d_Ω represents the signed distance function (SDF) with value

$$d_\Omega(x) = \begin{cases} d(x, \partial\Omega) & \text{if } x \in \Omega \\ 0 & \text{if } x \in \partial\Omega \\ -d(x, \partial\Omega) & \text{if } x \in \bar{\Omega}^c, \end{cases} \quad (12)$$

where the Euclidian distance of $x \in \mathbb{R}^d$ to a closed set $K \subset \mathbb{R}^d$ is defined as

$$d(x, K) = \min_{y \in K} \|x - y\|_2 \quad (13)$$

for Euclidian distance $\|\cdot\|_2$. The latter penalty can be justified by arguing, that an increased thinness would be undesirable with regards to the durability of the optimized shape. From a shape computational viewpoint, it ensures staying in the associated shape space. In numerics it prevents intersections of line segments, which may cause a breakdown of the optimization algorithm. In this light, we only take into account the positive part of the SDF of the offset value. Hence, we define for a real-valued function $f : \Omega \rightarrow \mathbb{R}$ the positive part as

$$f^+ = \max(f(x), 0) = \begin{cases} f(x) & \text{if } f(x) > 0 \\ 0 & \text{otherwise} \end{cases}. \quad (14)$$

Finally, we would like to point out, that the objective is controlled by parameters $\nu_1, \nu_2, \nu_3, \nu_4$ and ν_5 which need to be defined a priori (for further details cf. to Section 4).

Remark. The volume penalization could also be replaced by a geometrical constraint to meet a certain voluminous value, e.g. the initial size of the obstacle

$$\int_{\Omega} 1 \, dx = \text{vol}(\Omega) = \text{vol}(\Omega_0) = \int_{\Omega_0} 1 \, dx.$$

This approach would call for a different algorithmic handle, e.g. in [12] an augmented Lagrangian is proposed.

3 Derivation of the Shape Derivative

We now fix notations and definitions in the first part, before deriving the adjoint equations and shape derivatives in the second part, that are necessary to solve the PDE-constrained optimization problem.

3.1 Notations and Definitions

The idea of shape optimization is to deform an object ideally to minimize some target functional. Hence, to find a suitable way of deforming we are interested in some shape analogy to classical derivatives. Here we use a methodology that is commonly used in shape optimization, extensively elaborated in various works [7][8][9].

In this section we fix notations and definitions following [11][12], amending whenever it appears necessary. We start by introducing a family of mappings $\{\phi_\epsilon\}_{\epsilon \in [0, \tau]}$ for $\tau > 0$ that are used to map each current position $x \in \Omega$ to another by $\phi_\epsilon(x)$, where we choose the vector field \vec{V} as the direction for the so-called perturbation of identity

$$x_\epsilon = \phi_\epsilon(x) = x + \epsilon \vec{V}(x). \quad (15)$$

According to this methodology, we can map the whole domain Ω to another Ω_ϵ such that

$$\Omega_\epsilon = \{x_\epsilon | x + \epsilon \vec{V}(x), x \in \Omega\}. \quad (16)$$

We define the Eulerian Derivative as

$$DJ(\Omega)[\vec{V}] = \lim_{\epsilon \rightarrow 0^+} \frac{J(\Omega_\epsilon) - J(\Omega)}{\epsilon}. \quad (17)$$

Commonly, this expression is called shape derivative of J at Ω in direction \vec{V} and in this sense J shape differentiable at Ω if for all directions \vec{V} the Eulerian derivative exists and the mapping $\vec{V} \mapsto DJ(\Omega)[\vec{V}]$ is linear and continuous. In addition, we define the material derivative of some scalar function $p : \Omega \rightarrow \mathbb{R}$ at $x \in \Omega$ by the derivative of a composed function $p_\epsilon \circ \phi_\epsilon : \Omega \rightarrow \Omega_\epsilon \rightarrow \mathbb{R}$ for $p_\epsilon : \Omega_\epsilon \rightarrow \mathbb{R}$ as

$$D_m p(x) := \lim_{\epsilon \rightarrow 0^+} \frac{p_\epsilon \circ \phi_\epsilon(x) - p(x)}{\epsilon} = \frac{d}{d\epsilon} (p_\epsilon \circ \phi_\epsilon)(x) \Big|_{\epsilon=0^+} \quad (18)$$

and the corresponding shape derivative for a scalar p and a vector-valued \vec{P} for which the material derivative is applied component-wise as

$$Dp[\vec{V}] := D_m p - \vec{V} \cdot \nabla p \quad (19)$$

$$D\vec{P}[\vec{V}] := D_m \vec{P} - \vec{V}^T \nabla \vec{P}, \quad (20)$$

where the distinction is that ∇p is the gradient of a scalar and $\nabla \vec{P}$ is the tensor derivative of a vector. In the following, we will use the abbreviation \dot{p} and $\dot{\vec{P}}$ to mark the material derivative of p and \vec{P} . In Section 3 we will need to have the following calculation rules on board [21]

$$D_m(pq) = D_m p q + p D_m q \quad (21)$$

$$D_m \nabla p = \nabla D_m p - \nabla \vec{V}^T \nabla p \quad (22)$$

$$D_m \nabla \vec{P} = \nabla D_m \vec{P} - \nabla \vec{V}^T \nabla \vec{P} \quad (23)$$

$$D_m(\nabla q^T \nabla p) = \nabla D_m p^T \nabla q - \nabla q^T (\nabla \vec{V} + \nabla \vec{V}^T) \nabla p + \nabla p^T \nabla D_m q. \quad (24)$$

In addition, the basic idea in the proof of the shape derivative in the next section will be to pull back each integral defined on the transformed field back to the original configuration. We therefore need to state the following rule for differentiating domain integrals [21]

$$\frac{d}{d\epsilon} \left(\int_{\Omega_\epsilon} p_\epsilon \, dx_\epsilon \right) \Big|_{\epsilon=0^+} = \int_{\Omega} (D_m p + \nabla \cdot \vec{V} p) \, dx. \quad (25)$$

3.2 Shape Derivative

From the discussion above, we define the derivative of some functional with respect to Ω in the \vec{V} direction that explicitly and implicitly depends on the domain $j(\Omega, u(\Omega))$ by

$$Dj(\Omega, u(\Omega))[\vec{V}] = \frac{d}{d\epsilon} j(\Omega_\epsilon, u(\Omega_\epsilon)) \Big|_{\epsilon=0} = D_1 j(\Omega, u(\Omega))[\vec{V}] + D_2 j(\Omega, u(\Omega)) \dot{u}, \quad (26)$$

where

$$\dot{u} = \frac{d}{d\epsilon} u(\Omega_\epsilon)|_{\epsilon=0}. \quad (27)$$

The idea is to circumvent the derivative of u , which would imply one problem for each direction of \vec{V} by solving an auxiliary problem [10].

Before defining this problem, we take care of the constraints (1) and formulate the Lagrangian

$$\mathcal{L}(\Omega, U, P) = J_{1,2}(\Omega) + a(U, P) - b(P), \quad (28)$$

where $J_{1,2}(\Omega) = J_1(\Omega) + J_2(\Omega)$ consists of the first two objectives (7)-(8), and $a(U, P)$ and $b(P)$ are obtained from the boundary value problem (1). We rewrite the equations in weak form by multiplying with some arbitrary test function $P \in H^1(\Omega \times (0, T))^3$ obtaining the form $a(U, P) = a(H, \vec{Q}, p, \vec{R})$

$$\begin{aligned} a(H, \vec{Q}, p, \vec{R}) := & \int_0^T \int_\Omega \left[\frac{\partial H}{\partial t} + \nabla \cdot \vec{Q} \right] p \, dx \, dt \\ & + \int_0^T \int_\Omega \left[\frac{\partial \vec{Q}}{\partial t} + \nabla \cdot \left(\frac{\vec{Q}}{H} \otimes \vec{Q} + \frac{1}{2} g H^2 \mathbf{I}_2 \right) \right] \cdot \vec{R} \, dx \, dt \\ & + \int_0^T \int_\Omega \mu_v \nabla(H + z) \cdot \nabla p \, dx \, dt - \int_0^T \int_{\Gamma_2} \mu_v \nabla(H_1 + z) \cdot \vec{n} p \, ds \, dt \\ & + \int_0^T \int_\Omega G(\mu_f) \nabla \vec{Q} : \nabla \vec{R} \, dx \, dt + \int_0^T \int_\Omega g H \nabla z \cdot \vec{R} \, dx \, dt \end{aligned} \quad (29)$$

and a zero perturbation term.

Remark. For readability we left out the friction term, however up to some repetitive use of chain and product rule the handling stays the same as for the variations in the bed slope.

Remark. Here and in what follows we assume the flow to be free of discontinuities, e.g. induced by a discontinuous bottom profile z or wave height H , which would prohibit us from performing adjoint-sensitivity analyses and ensuring the requirements in Theorem 1 and 2.

Remark. To continue with adjoint calculations and to enforce initial and boundary conditions we are required to integrate by parts on the derivative-containing terms.

We obtain state equations from differentiating the Lagrangian with respect to P and the auxiliary problem, the adjoint equations, from differentiating the Lagrangian with respect to the states U . The adjoint is formulated in the following theorem:

Theorem 1. (Adjoint) Assume that the parabolic PDE problem (1) is H^1 -regular, so that its solution U is at least in $H^1(\Omega \times (0, T))^3$. Then the adjoint in strong form (without friction term) is given by

$$\begin{aligned} -\frac{\partial p}{\partial t} + \frac{1}{H^2} (\vec{Q} \cdot \nabla) \vec{R} \cdot \vec{Q} - g H (\nabla \cdot \vec{R}) - \nabla \cdot (\mu_v \nabla p) + g \nabla z \cdot \vec{R} &= -\nu_1 (E \sigma_\alpha)_{H, \Gamma_1, \tilde{T}} \\ -\frac{\partial \vec{R}}{\partial t} - \nabla p - \frac{1}{H} (\vec{Q} \cdot \nabla) \vec{R} - \frac{1}{H} (\nabla \vec{R})^T \vec{Q} - \nabla \cdot (G(\mu_f) \nabla \vec{R}) &= -\nu_2 (\vec{Q})_{\Gamma_1} \end{aligned} \quad (30)$$

where we have on $\Gamma_1 \times \tilde{T}$

$$(E \sigma_\alpha)_{H, \Gamma_1, \tilde{T}} = 2 \frac{E}{H} \sigma_\alpha (H - H_{cr}) + E \sigma_\alpha (H - H_{cr}) (1 - \sigma_\alpha (H - H_{cr})) \quad (31)$$

such as final time conditions

$$\begin{aligned} p &= 0 \quad \text{in } \Omega \times \{T\} \\ \vec{R} &= 0 \quad \text{in } \Omega \times \{T\} \end{aligned} \quad (32)$$

and boundary conditions

$$\begin{aligned} \vec{R} \cdot \vec{n} &= 0, \nabla p \cdot \vec{n} = 0, \nabla \vec{R}_1 \cdot \vec{n} = 0, \nabla \vec{R}_2 \cdot \vec{n} = 0 \quad \text{on } \Gamma_1, \Gamma_3 \times (0, T) \\ p \vec{n} + \frac{1}{H_1} (\vec{Q} \cdot \vec{n}) \vec{R} + \frac{1}{H_1} (\vec{Q} \vec{R}) \cdot \vec{n} &= 0, \nabla \vec{R}_1 \cdot \vec{n} = 0, \nabla \vec{R}_2 \cdot \vec{n} = 0 \quad \text{on } \Gamma_2 \times (0, T). \end{aligned} \quad (33)$$

Proof. See Appendix A □

The obtained adjoint equations can be written in vector form as

$$-\frac{\partial P}{\partial t} + AP_x + BP_y + CP - \nabla \cdot (G(\mu)\nabla P) = S, \quad (34)$$

where

$$A = \begin{pmatrix} 0 & \frac{Q_1}{H^2} - gH & \frac{Q_1 Q_2}{H^2} \\ -1 & -2\frac{Q_1}{H} & -\frac{Q_2}{H} \\ 0 & 0 & -\frac{Q_1}{H} \end{pmatrix}, \quad B = \begin{pmatrix} 0 & \frac{Q_1 Q_2}{H^2} & \frac{Q_2^2}{H^2} - gH \\ 0 & -\frac{Q_2}{H} & 0 \\ -1 & -\frac{Q_1}{H} & -2\frac{Q_2}{H} \end{pmatrix} \quad (35)$$

and C originates from variations in the sediment in (3) such that

$$C = \begin{pmatrix} 0 & g\frac{\partial z}{\partial x} & g\frac{\partial z}{\partial y} \\ 0 & 0 & 0 \\ 0 & 0 & 0 \end{pmatrix}. \quad (36)$$

Finally, S corresponds to the right hand-side of (30).

Remark. If one desires to include additional sources, e.g. accounting for sediment friction, C from (36) would need to be adjusted.

Remark. Shape derivatives can for a sufficiently smooth domain be described via boundary formulations using Hadamard's structure theorem [8]. The integral over Ω is then replaced by an integral over Γ_3 that acts on the associated normal vector. In this paper, we will only consider the volume form, which will be then used to obtain smooth mesh deformations from a Riesz projection of this shape derivative.

Theorem 2. (*Shape Derivative*) Assume that the parabolic PDE problem (1) is H^1 -regular, so that its solution U is at least in $H^1(\Omega \times (0, T))^3$. Moreover, assume that the adjoint equation (30) admits a solution $P \in H^1(\Omega \times (0, T))^3$. Then the shape derivative of the objectives $J_{1,2}$ (without friction term) at Ω in the direction \vec{V} is given by

$$\begin{aligned} DJ_{1,2}(\Omega)[\vec{V}] = & \int_0^T \int_{\Omega} \left[-(\nabla \vec{V})^T : \nabla \vec{Q} p - (\nabla \vec{V})^T : \nabla \vec{Q} \frac{\vec{Q}}{H} \cdot \vec{R} - (\nabla \vec{V} \vec{Q} \cdot \nabla) \frac{\vec{Q}}{H} \cdot \vec{R} \right. \\ & - gH(\nabla \vec{V})^T \nabla H \cdot \vec{R} - \mu_v \nabla(H+z)^T (\nabla \vec{V} + \nabla \vec{V}^T) \nabla p \\ & - G(\mu_f) \nabla \vec{Q} \nabla \vec{V} : \nabla \vec{R} - G(\mu_f) \nabla \vec{Q} \nabla \vec{V}^T : \nabla \vec{R} \\ & - gH \nabla \vec{V}^T \nabla z \cdot \vec{R} + \operatorname{div}(\vec{V}) \left\{ \frac{\partial H}{\partial t} p + \nabla \cdot \vec{Q} p + \frac{\partial \vec{Q}}{\partial t} \cdot \vec{R} \right. \\ & + (\vec{Q} \cdot \nabla) \frac{\vec{Q}}{H} \cdot \vec{R} + \nabla \cdot \vec{Q} \frac{\vec{Q}}{H} \cdot \vec{R} + \frac{1}{2} g \nabla H^2 \cdot \vec{R} + gH \nabla z \cdot \vec{R} \\ & \left. \left. + \mu_v \nabla(H+z) \cdot \nabla p + G(\mu_f) \nabla \vec{Q} : \nabla \vec{R} \right\} \right] dx dt. \end{aligned} \quad (37)$$

Proof. See Appendix B □

The shape derivatives of the penalty terms (volume, perimeter and thickness) are obtained as, see e.g. [8][22]

$$DJ_3(\Omega)[\vec{V}] = \nu_3 \int_{\Omega} -\nabla \cdot \vec{V} dx \quad (38)$$

$$DJ_4(\Omega)[\vec{V}] = \nu_4 \int_{\Gamma_3} \kappa_m \langle \vec{V}, \vec{n} \rangle ds \quad (39)$$

and see [20] for

$$\begin{aligned} DJ_5(\Omega)[\vec{V}] = & \nu_5 \int_{\Gamma_3} \int_0^{d_{min}} \left[\vec{V}(x) \cdot \vec{n}(x) \left\{ \kappa_m(x) (d_{\Omega}(x_m))^+{}^2 \right. \right. \\ & \left. \left. + 2d_{\Omega}(x_m)^+ \nabla d_{\Omega}(x_m) \cdot \nabla d_{\Omega}(x) \right\} \right. \\ & \left. \left. - \vec{V}(p_{\partial\Omega}(x_m)) \cdot \vec{n}(p_{\partial\Omega}(x_m)) 2(d_{\Omega}(x_m))^+ \right] d\xi ds \end{aligned} \quad (40)$$

for mean curvature κ_m , and offset point $x_m = x - \xi \vec{n}(x)$, where we require the shape derivative of the SDF [20]

$$Dd_\Omega(x)[\vec{V}] = -\vec{V}(p_{\partial\Omega}(x)) \cdot \vec{n}(p_{\partial\Omega}(x)) \quad (41)$$

with operator $p_{\partial\Omega}$ that projects a point $x \in \Omega$ onto its closest boundary and holds for all $x \notin \Sigma$, where Σ is referred to as the ridge, where the minimum in (13) is obtained by two distinct points.

4 Numerical Results

We now first discuss the implementation in detail, before applying these techniques to selected examples in the following subsections.

4.1 Implementation Details

We rely on the classical structure of adjoint-based shape optimization algorithms shortly sketched in the algorithm below. The solution to the SDF in (11) is mesh dependent. For a mesh with undiscretized obstacle the SDF is approximated

Algorithm 1: Shape Optimization Algorithm

Initialization

while $\|DJ(\Omega_k)[\vec{V}]\| > \epsilon_{TOL}$ **do**

1. Calculate SDF w_k [via AABBT]

2. Calculate State U_k [via (42)]

3. Calculate Adjoint P_k [via (42)]

4. Calculate Gradient W_k [via $DJ_{1,2,3,4,5}(\Omega)[\vec{V}]$ & Linear Elasticity (56)]

5. Perform Linesearch for \tilde{W}_k

6. Calculate Ω_{k+1} [via \tilde{W}_k and (16)]

end while

based on axes-aligned-bounding-boxes trees (AABBT) [23] on a background mesh. We refer to Figure 3 for an exemplifying visualization. Note, we have highlighted the initial boundary mesh points in red, exemplifying offset points in blue such as mesh and background mesh in the left figure and due to visibility, the distance of background nodes to the nearest exterior boundary point of the original mesh in the right figure.

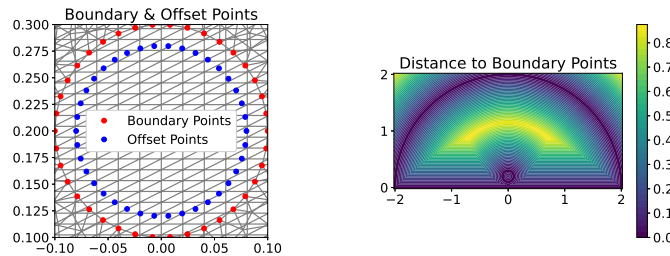


Figure 3: 1.: Boundary and Offset Points on Mesh and Background Mesh, 2.: Distance to Boundary Points via AABBT

We solve the boundary value problem (1), the adjoint problem (30) and the deformation of the domain with the help of the finite element solver FEniCS [23]. For the time discretization we can choose between implicit and explicit integration arising from theta-methods [24]. High accuracy even for the inviscid and hyperbolic PDE, i.e. $\mu = 0$, is achieved using a discontinuous Galerkin (DG) method to discretize in space [25][26][27]. This implies discontinuous cell transitions, and hence a formulation based on each element $\kappa \in \mathcal{T}_h$ or facet Γ_I for a subdivision \mathcal{T}_h of some domain Ω , such as a redefinition of each function and operator on the so-called broken and possibly vector-valued d -dimensional Sobolev space $\mathcal{H}^1(\mathcal{T}_h \times (0, T))^d$. In this light, we also need to define the average $\{\{U\}\} = (U^+ + U^-)/2$ and jump term $\llbracket U \rrbracket = U^+ \otimes n_+ + U^- \otimes n_-$ to express fluxes on cell transitions. The discretization then reads for solution and test-function U_h, P_h from some finite element approximation space of $\mathcal{H}^1(\mathcal{T}_h \times (0, T))^3$ for an SIPG scheme as

[28][29]

$$\begin{aligned}
F_h(U_h, P_h) = & \int_0^T \int_{\Omega} \left[\frac{\partial U_h}{\partial t} \cdot P_h - F(U_h) : \nabla_h P_h + G(\mu) \nabla_h(\hat{U}_h) : \nabla_h P_h \right. \\
& \left. - S(U_h) \cdot P_h \right] dx dt + \int_0^T \sum_{\kappa \in \mathcal{T}_h} \int_{\partial \kappa \setminus \Gamma} \mathcal{F}(U_h^+, U_h^-, \vec{n}) \cdot P_h^+ ds dt \\
& + \int_0^T \int_{\Gamma_I} \left[\underline{\delta}_h : \llbracket P_h \rrbracket - \{ \{ G(\mu) \nabla_h(P_h) \} \} : \llbracket \hat{U}_h \rrbracket \right. \\
& \left. - \{ \{ G(\mu) \nabla_h(\hat{U}_h) \} \} : \llbracket P_h \rrbracket \right] ds dt + N_{\Gamma, h}(U_h, P_h) = 0,
\end{aligned} \tag{42}$$

where the numerical flux function $\mathcal{F}(U_h^+, U_h^-, \vec{n})$ defines the fluxes at the discontinuous cell transitions, incorporating specific quantities at the respective boundaries. For the advective flux and for a given flux Jacobian $\mathcal{J}_i := \partial_U F_i(U)$ and matrix $B(U, \vec{n}) = \sum_{i=1}^2 n_i \mathcal{J}_i(U)$ we can choose between a variety of numerical fluxes [25], e.g.

(Local) Lax-Friedrichs Flux:

$$\mathcal{F}_1(U^+, U^-, \vec{n})|_{\partial \kappa} = \frac{1}{2} (F(U^+) \cdot \vec{n} + F(U^-) \cdot \vec{n} + \alpha_{\max}(U^+ - U^-)), \tag{43}$$

where $\alpha_{\max} = \max_{V=U^+, U^-} \{ |\lambda(B(V, \vec{n}_\kappa))| \}$ with $\lambda(B(V, \vec{n}_\kappa))$ returning a sequence of eigenvalues for the matrix B restricted on a side of element κ .

HLLE Flux:

$$\mathcal{F}_2(U^+, U^-, \vec{n})|_{\partial \kappa} = \frac{1}{\lambda^+ - \lambda^-} (\lambda^+ F(U^+) \cdot \vec{n} - \lambda^- F(U^-) \cdot \vec{n} - \lambda^+ \lambda^- (U^+ - U^-)), \tag{44}$$

where $\lambda^+ = \max(\alpha_{\max}, 0)$ and $\lambda^- = \min(\alpha_{\min}, 0)$, for α_{\min} defined in accordance with α_{\max} . The required SWE Jacobian is written as

$$\mathcal{J}_1(U) = \begin{pmatrix} 0 & 1 & 0 \\ -\frac{Q_1^2}{H^2} + gH & 2\frac{Q_1}{H} & 0 \\ -\frac{Q_1 Q_2}{H^2} & \frac{Q_2}{H} & \frac{Q_1}{H} \end{pmatrix} \quad \mathcal{J}_2(U) = \begin{pmatrix} 0 & 0 & 1 \\ -\frac{Q_1 Q_2}{H^2} & \frac{Q_2}{H} & \frac{Q_1}{H} \\ -\frac{Q_2^2}{H^2} + gH & 0 & 2\frac{Q_2}{H} \end{pmatrix}. \tag{45}$$

Hence, we obtain the following eigenvalues, where $c = \sqrt{gH}$ denotes the wave celerity [25]

$$\begin{aligned}
\lambda(n_1 \mathcal{J}_1 + n_2 \mathcal{J}_2) &= \{\lambda_1, \lambda_2, \lambda_3\} \\
&= \{un_1 + vn_2 - c, un_1 + vn_2, un_1 + vn_2 + c\}.
\end{aligned} \tag{46}$$

Remark. From (46) also the hyperbolicity for the shallow water system is obtained, i.e. $\lambda_i \in \mathbb{R}$ for $i \in \{1, \dots, 3\}$. In addition if $c \neq 0$ or $H > 0$, we obtain distinct eigenvalues, which lead to strict hyperbolicity.

Remark. For a mesh with discretized obstacle and suitable transitional boundaries the SDF can be based on the solution of the diffusive Eikonal Equation with $f(x) = 1, q(x) = 0$

$$\begin{aligned}
|\nabla w(x)| - \mu_{SDF} \Delta w(x) &= f(x) & x \in \Omega \\
w(x) &= q(x) & x \in \partial \Omega,
\end{aligned} \tag{47}$$

written in weak form as

$$\int_{\Omega} \sqrt{\nabla w \cdot \nabla w} v dx - \int_{\Omega} f v dx + \int_{\Omega} \mu_{SDF} \nabla w \cdot \nabla v dx = 0, \tag{48}$$

where $w \in H^1(\Omega)$ for all $v \in H^1(\Omega)$ and $\mu_{SDF} = \max_i h_i$ is dependent on the cell-diameter h_i for the i^{th} cell $\kappa_i \subset \Omega$ for $i \in \{1, \dots, m\}$. In this setting, the diffusive Eikonal equation can serve as an additional constraint to (6) and be considered in adjoint-based shape optimization.

Remark. In the presence of sources, especially for a discontinuous sediment z , a well-balanced numerical scheme is only obtained by methods of flux balancing. For this, the method presented in [30] is extended to two dimensions. In addition, diffusive terms introduced in (1) cancel naturally in still water conditions. Finally respectively (43) and (44) are redefined.

In (42) we define the penalization term for the viscous fluxes as

$$\underline{\delta}_h(\hat{U}_h) = C_{IP} \frac{k^2}{h} \{ \{ G(\mu) \} \} \llbracket \hat{U}_h \rrbracket, \quad (49)$$

where $C_{IP} > 0$ is a constant, $k > 0$ the polynomial order of the DG method and $h > 0$ the ratio of the cell volume and the facet area. What is remaining in (42) is the specification of the boundary term, here we state that

$$\begin{aligned} N_{\Gamma,h}(U_h, P_h) &= \int_0^T \int_{\Gamma} \mathcal{F}(U_h^+, U_{\Gamma}(U_h^+), \vec{n}) \cdot P_h^+ \, ds \, dt \\ &+ \int_0^T \int_{\Gamma_N} \left[\underline{\delta}_{\Gamma}(\hat{U}_h^+) : P_h \otimes \vec{n} + G(\mu^+) \nabla_h(\hat{U}_h^+) : P_h^+ \otimes \vec{n} \right. \\ &\quad \left. - G(\mu^+) \nabla_h V_h^+ : (\hat{U}_h^+ - U_{\Gamma}(\hat{U}_h^+)) \otimes \vec{n} \right] \, ds \, dt, \end{aligned} \quad (50)$$

where Γ_N are all boundaries of type Neumann. Additionally, we define

$$\underline{\delta}_{\Gamma}(U_h^+) = C_{IP} G(\mu^+) \frac{k^2}{h} (U_h^+ - U_{\Gamma}(U_h^+)) \otimes \vec{n} \quad (51)$$

$$\mathcal{F}(U_h^+, U_{\Gamma}(U_h^+), \vec{n}) = \frac{1}{2} [\vec{n} \cdot F(U_h^+) + \vec{n} \cdot F(U_{\Gamma}(U_h^+))]. \quad (52)$$

For the pure advective SWE open and rigid-wall boundary functions are defined as in [25]. Having obtained a discretized solution for the forward problem, we calculate the SWE adjoint problem in the same manner using a DG discretization in space and a member of the theta-method for the time discretization. For this we rewrite the vector form of the SWE adjoint (34) with the help of the product rule, i.e.

$$\frac{\partial P}{\partial t} - \nabla \cdot (AP, BP) - \tilde{C}P + \nabla \cdot (G(\epsilon) \nabla P) = -S, \quad (53)$$

where \tilde{C} is defined to be

$$\tilde{C} = C - A_x - B_y. \quad (54)$$

The following theorem provides us then with the necessary eigenvalues of the adjoint flux Jacobian $\mathcal{J}_i^* := \partial_P F_i^*(P) = -\partial_P(AP, BP)$.

Theorem 3. (Eigenvalues of the Adjoint Flux Jacobian) *The eigenvalues of matrix $B^*(P, \vec{n})$ belonging to the adjoint flux Jacobian $\mathcal{J}_i^* := \partial_P F_i^*(P)$ equal the eigenvalues of matrix $B(U, \vec{n})$ belonging to the flux Jacobian $\mathcal{J}_i := \partial_U F_i(U)$.*

Proof.

$$\lambda(B(U, \vec{n})) = \lambda\left(\sum_{i=1}^2 \vec{n}_i \partial_U F_i(U)\right) = \lambda\left(\sum_{i=1}^2 n_i \partial_P F_i^*(P)\right) = \lambda(B^*(P, \vec{n})) \quad (55)$$

since $\sum_{i=1}^2 n_i \partial_U F_i(U) = \sum_{i=1}^2 n_i \partial_P F_i^*(P)^T$ which is due to the linearity of the adjoint system. The determinant-invariance of the transpose-operator then leads to the assertion. \square

Remark. The theorem above also provides us with hyperbolicity for the adjoint system. However, the linearity would essentially enable us to solve the system with less expensive methods, which could result in less degrees of freedom. We furthermore highlight that Theorem 3 provides us with stability of the numerical scheme for the adjoint equations as well, e.g. if we have chosen the time steps in accordance with the CFL-condition for explicit time-integration in the forward problem.

Updating the finite element mesh in each iteration is done via the solution $\vec{W} : \Omega \rightarrow \mathbb{R}^2$ of the linear elasticity equation [11]

$$\begin{aligned} \int_{\Omega} \sigma(\vec{W}) : \epsilon(\vec{V}) \, dx &= DJ(\Omega)[\vec{V}] & \forall \vec{V} \in H_0^1(\Omega, \mathbb{R}^2) \\ \sigma &:= \lambda_{elas} Tr(\epsilon(\vec{W}))I + 2\mu_{elas} \epsilon(\vec{W}) \\ \epsilon(\vec{W}) &:= \frac{1}{2}(\nabla \vec{W} + \nabla \vec{W}^T) \\ \epsilon(\vec{V}) &:= \frac{1}{2}(\nabla \vec{V} + \nabla \vec{V}^T), \end{aligned} \quad (56)$$

where σ and ϵ are called strain and stress tensor and λ_{elas} and μ_{elas} are called Lamé parameters. In our calculations we have chosen $\lambda_{elas} = 0$ and μ_{elas} as the solution of the following Poisson problem

$$\begin{aligned} -\Delta \mu &= 0 & \text{in } \Omega \\ \mu &= \mu_{max} & \text{on } \Gamma_3 \\ \mu &= \mu_{min} & \text{on } \Gamma_1, \Gamma_2. \end{aligned} \quad (57)$$

The source term $DJ(\Omega)[\vec{V}]$ in (56) consists of a volume and surface part, i.e. $DJ(\Omega)[\vec{V}] = DJ_\Omega[\vec{V}] + DJ_{\Gamma_3}[\vec{V}]$. Here the volumetric share comes from our SWE shape derivative w.r.t. the first two objectives and the penalty on the volume, where we only assemble for test vector fields whose support intersects with the interface Γ_3 and is set to zero for all other basis vector fields [22]. The surface part comes from the parameter regularization and the minimum thinness penalty (11), where we have implemented the numerical attractive equivalent formulations

$$DJ_4(\Omega)[\vec{V}] = \nu_4 \int_{\Gamma_3} \left[\nabla \cdot \vec{V} - \left\langle \frac{\partial \vec{V}}{\partial \vec{n}}, \vec{n} \right\rangle \right] ds \quad (58)$$

and

$$\begin{aligned} DJ_5(\Omega)[\vec{V}] &= \nu_5 \int_{\Gamma_3} \int_0^{d_{min}} \left[\vec{V} \cdot \left\{ \nabla (d_\Omega(x_m)^+)^2 \right\} - \left\langle \nabla (d_\Omega(x_m)^+)^2, \vec{n} \right\rangle \vec{n} \right] \\ &\quad + (d_\Omega(x_m)^+)^2 \left\{ \nabla \cdot \vec{V} - \left\langle \frac{\partial \vec{V}}{\partial \vec{n}}, \vec{n} \right\rangle \right\} \\ &\quad + \vec{V} \cdot \vec{n} \left\{ 2d_\Omega(x_m)^+ \nabla d_\Omega(x_m) \cdot \vec{n} \right\} \\ &\quad - \vec{V} \cdot (p_{\partial\Omega}(x_m)) \cdot \vec{n} (p_{\partial\Omega}(x_m)) 2(d_\Omega(x_m))^+ \Big] d\xi ds. \end{aligned} \quad (59)$$

In order to guarantee the attainment of useful shapes, which minimize the objective, a backtracking line search is used, which limits the step size in case the shape space is left [22], i.e. having intersecting line segments or in the case of a non-decreasing objective evaluation. As described in the algorithm before, the iteration is finally stopped if the norm of the shape derivative has become sufficiently small.

4.2 Ex.1: The Half-Circled Mesh

In the first example, we will look at the model problem - the half circle that was described in Section 2. The associated mesh is displayed in Figure 4 and was created using the finite element mesh generator GMSH [31], we have meshed finer around the obstacle to ensure a high resolution. We set Gaussian initial conditions as $\hat{U}_0 = (1 + \exp(-15x^2 - 15(y-1)^2), 0, 0)$, which result in a wave travelling in time towards the boundaries. As before, we interpret $\Gamma_1, \Gamma_2, \Gamma_3$ as coastline, open sea and obstacle boundary. Accordingly, we prescribe the boundary conditions using rigid-wall conditions on Γ_1, Γ_3 and outflow boundaries on Γ_2 . The parameters in the shallow water system are set as follows: For the weight of the diffusion terms in the momentum equation we set $\mu_f = (0.01, 0.01)$ and determine μ_v by the usage of the mentioned shock detector [17]. The gravitational acceleration is fixed at roughly 9.81 and the parameter K in Manning's formula is at 0.049 for a sandy beach. Our calculations are performed for two test cases - a linear decreasing bottom $z = 0.5 - 0.25y$ and a non-flat bottom determined by a Gaussian peak $z = \exp(-6(x-0.5)^2 - 6(y-0.2)^2)$, as displayed in Figure 4. We are targeting a minimal mechanical wave energy for waves above the water's rest height, such that the energy and sigmoid function are defined in terms of $H + z$ for threshold $H_{cr} = 1$ and slope parameter $\alpha = 10$ such as zeroed velocities by setting $\nu_1 = \nu_2 = 1$. In addition, we penalize volume and thinness by setting $\nu_3 = 1e-4, \nu_5 = 1e-2$ such as enforcing a stronger regularization by $\nu_4 = 1e-4$. In this example we have used an implicit backward Euler time-scheme and a DG-method of first order that was described before. For the spatial discretization, we have used the HLLE-flux function for the convective terms and $C_{IP} = 20$ in the SIPG method. Solving the state equations requires the definition of the time-horizon, e.g. as $\tilde{T} = (0, T) = (0, 2.5)$, which is chosen to include one full wave period, i.e. the travel of a wave to and from the shore. The discretization in time is based on a step size of $dt = 5e-3$. Due to the nonlinear nature of the SWE we have used a Newton solver, where we set the absolute and relative tolerance as $\epsilon_{abs} = \epsilon_{rel} = 1e-6$. The solution of the adjoint problem follows likewise, but stepping backwards in time. Since the problem is linear, a Newton solver is no longer needed. Having solved state and adjoint equations the mesh deformation is performed as described, where we specify $\mu_{min} = 10$ and $\mu_{max} = 100$ in (57). The step size is at $\rho = 1$ and shrinks whenever criteria for line searches are not met. In Figure 5 results of the shape optimization are displayed, firstly for a linear and secondly a Gaussian bottom after 44 and 33 steps of optimization.

The deformations are symmetric in the first and in the opposing direction of the sediment hill in the second case. As we observe in the lower part of Figure 5, we have achieved notable decreases in the objective.

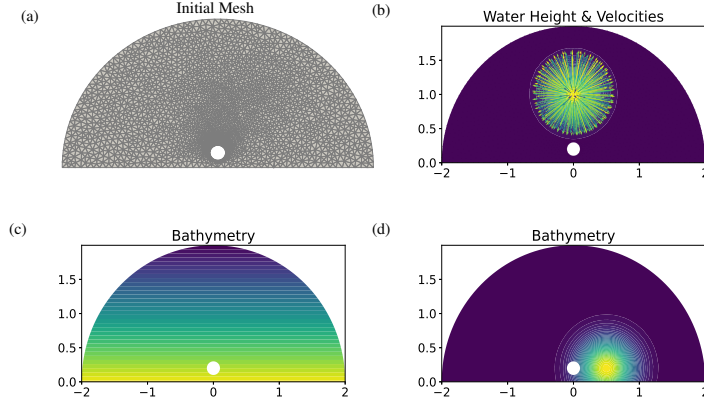


Figure 4: (a) Initial Mesh and Obstacle, (b) Field State at $t = 0.1$, (c) Linear Bathymetry, (d) Gaussian Peak Bathymetry

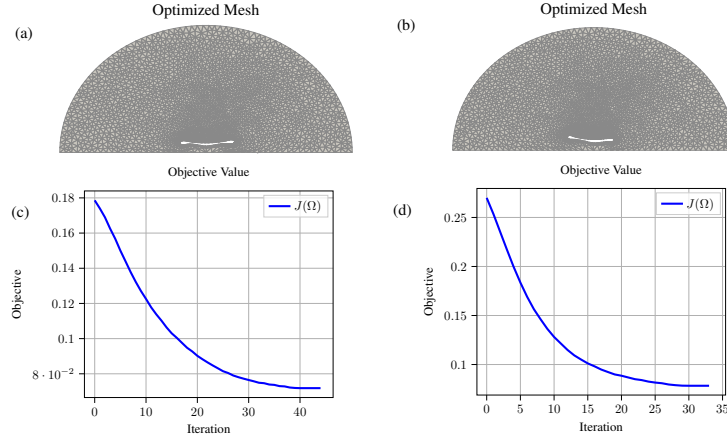


Figure 5: (a) Optimized Obstacle for Linear Seabed, (b) Optimized Obstacle for Gaussian Seabed, (c) Objective for Linear Seabed, (d) Objective for Gaussian Seabed

4.3 Ex.2: Langue de Barbarie

A more realistic computation is performed in the second example. Here we look at the LdB a coastal section in the north of Dakar, Senegal. In 1990 it consisted of a long offshore island, which eroded in three parts within two decades. Waves now travel unhindered to the mainlands, which causes severe damage and already destroyed large habitats. Adjusting our model to this specific coastal section starts on mesh level. Shorelines are taken from the free GSHHG¹ databank, following [32]. We build up an interface from a geographical information system (QGIS3) for processing the data to a computer aided design software (GMSH) for the mesh generation. Similar to the preceding example, we interpret Γ_1 as coastline of the mainland, Γ_2 as the open sea boundary such as Γ_3 as the three offshore islands (cf. to Figure 7,8).

As before, we start with Gaussian initial conditions for the height of the water. Sediment data is taken from the GEBCO² databank, where bathymetric elevation is mapped to a mesh point using a nearest neighbors algorithm. The sediment elevation can be taken from Figure 6, while the wave propagation can be extracted from Figure 7. The remaining model-settings are similar to Section 4.2. Figure 8 pictures initial, such as deformed mesh and obstacle after 30 steps of optimization.

¹<https://www.ngdc.noaa.gov/mgg/shorelines/>

²<https://www.gebco.net/>

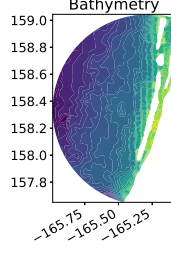


Figure 6: LdB Sediment Elevation

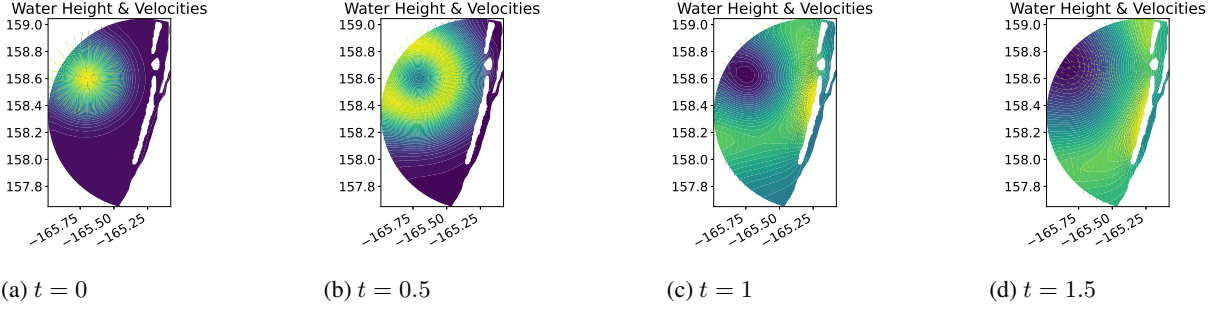
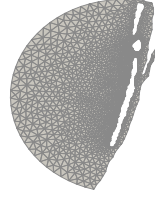
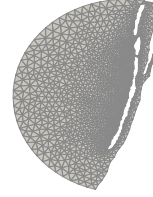


Figure 7: Visualization of a Wave Described by Height and Velocities, Travelling Towards the Shore for Initial Obstacle.



(a) Initial Mesh



(b) Optimized Mesh

Figure 8: Initial and Optimized Mesh and Obstacle

One can observe a similar behaviour as in Subsection 4.2, where the obstacle is stretched to protect an as large as possible area. In this setting, the optimizer suggests to reconnect the three islands. However, rebuilding the complete island would either call for a remeshing procedure or an alternative algorithm for shape optimization, e.g. level sets as in [3] are capable of similar. We highlight that obtained results must be treated with caution, since rebuilding would require an excessive amount of landmass. As an alternative, simulations with artificial offshore islands subject to volume constraints can be performed. In Figure 9 the convergence of the objective can be observed.

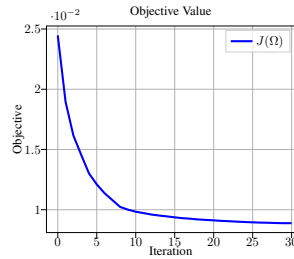


Figure 9: Objective for LdB Mesh

4.4 Ex.3: World Mesh

In the third and last example, we extend presented techniques to immersed-manifolds, in order to perform global shore protection. For this, we define Ω to be a smooth m -dimensional manifold immersed in R^n , where $m = 2$ denotes the topological dimension and $n = 3$ the geometric dimension. We assume a similar setting as before, where Γ_1 represents the continent of Africa and Γ_2 the remaining coastal points. In addition, we have placed three initial circled obstacles with boundary Γ_3 in before the shore of West-Africa that serve as obstacle. From the implementational side we have



Figure 10: High Resolution World Mesh

again used the GSHHG databank to obtain coastal data and mapped the points to a PolarSphere in GMSH (cf. to Figure 10). For the discretization we follow [33], from which an extension of the FEniCS software to the scenario above stems from. We aim for a solution in the geometric space i.e. $U_h = (H_h, u_h H_h, v_h H_h, w_h H_h)$ relying on DG -elements, i.e. $DG_1 \times DG_3$, where we weakly enforce the vector-valued velocity to be in the spherical tangent space. Alternatively, we could solve in the mixed discrete Function Space $DG_1 \times RT_1$, where RT_1 denotes Raviar-Thomas finite elements, which lie in the tangent space simple from its construction. We define initial conditions in the geometric space as $U_0 = (2 + \exp(-c(x - x_0)^2 - c(y - y_0)^2 - c(z - z_0)^2), 0, 0, 0)$ for suitable coordinates (x_0, y_0, z_0) and constant c . In contrast to the examples before, open sea boundaries are not required any more, such that all boundaries are subject to rigid boundary conditions. The seabed is for simplicity assumed to be flat. The remaining model-settings are similar to Subsection 4.2. The wave propagation is visualized in Figure 11.

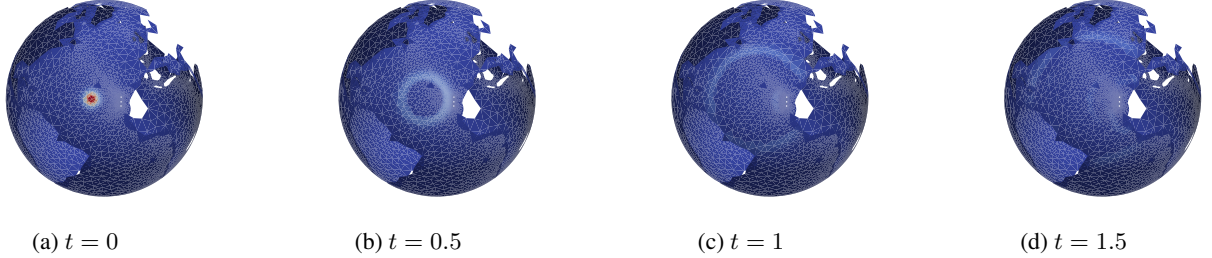


Figure 11: Visualization of a Wave Described by Height, Travelling Towards the Continents for Initial Obstacle.

For performing shape optimization we remark for completeness that updating the finite element mesh in each iteration is done via the solution $\vec{W} : \Omega \rightarrow \mathbb{R}^3$ of the linear elasticity equation, where we again enforce a tangential solution and hence solve

$$\int_{\Omega} \left[\sigma(\vec{W}) : \epsilon(\vec{V}) - l \vec{k} \cdot \vec{V} + \vec{W} \cdot \vec{k} \gamma \right] dx = DJ(\Omega)[\vec{V}]$$

$$\begin{aligned} \frac{\partial \vec{W}}{\partial \vec{n}} &= 0 & \text{on } \Gamma_3 \\ \vec{W} &= 0 & \text{on } \Gamma_1, \Gamma_2 \end{aligned} \quad (60)$$

for unit outward normal \vec{k} to the surface of the manifold, Lagrange multiplier $l \in DG_1$ for all (\vec{V}, γ) such as σ and ϵ as in (56). We would like to highlight that (60) represents an elliptic PDE, that can without further ado being solved directly. However, movements on a manifold would typically call for retractions, e.g. via usage of an exponential mapping [34, Chapter 4]. The resulting deformed obstacles can be seen in Figure 12.

In Figure 13 we once more observe convergence of the objective function.

Lastly, we would like to point out that the obtained results are only offering a simplistic analysis to protect the shore of Africa Γ_1 , that can be used as a first feasibility study. For a more comprehensive discussion one would need to adapt



Figure 12: Initial and Optimized Mesh and Obstacle

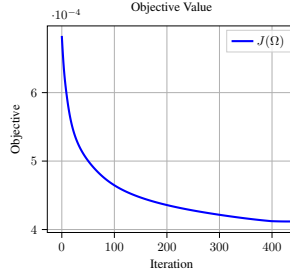


Figure 13: Objective for World Mesh

the model to non-shallow flows, simulate a non-flat seabed and take care on the wetting-drying phenomenon (cf. e.g. to [26]). On coastal boundaries Γ_1 , Γ_2 and Γ_3 more accurate solutions would be obtained by replacing rigid boundary conditions by partially absorbing boundary conditions. Finally, an extension of Γ_1 to all shores where various waves are produced with multiple obstacles placed before several shorelines, that are all restricted in volume, could lead to more sophisticated conclusions.

5 Conclusion

We have derived the time-dependent continuous adjoint and shape derivative of the SWE in volume form. The results were tested on a simplistic sample mesh for a linear and Gaussian seabed, as well as on more realistic meshes, picturing the Langue de Barbarie coastal section and a world simulation. The optimized shape strongly orients itself to the wave direction and to the mesh region that is to be protected. The results can be easily adjusted for arbitrary meshes, objective functions and different wave properties driven by initial and boundary conditions. However, the obtained obstacles are often too large for practical implementations, hence we admit that this work can only serve as a first feasibility study.

Keywords Shape Optimization · Obstacle Problem · Numerical Methods · Adjoint Methods · Shallow Water Equations · Coastal Erosion

Acknowledgement

This work has been supported by the Deutsche Forschungsgemeinschaft within the Priority program SPP 1962 "Non-smooth and Complementarity-based Distributed Parameter Systems: Simulation and Hierarchical Optimization". The authors would like to thank Diaraf Seck (Université Cheikh Anta Diop, Dakar, Senegal) and Mame Gor Ngom (Université Cheikh Anta Diop, Dakar, Senegal) for helpful and interesting discussions within the project Shape Optimization Mitigating Coastal Erosion (SOMICE).

References

- [1] Pascal Azerad, Benjamin Ivorra, Bijan Mohammad, and Frédéric Bouchette. *Optimal Shape Design of Coastal Structures Minimizing Coastal Erosion*. CIRM, 01 2005.

-
- [2] Damien Isebe, Pascal Azerad, Frédéric Bouchette, Benjamin Ivorra, and Bijan Mohammadi. Shape optimization of geotextile tubes for sandy beach protection. *International Journal for Numerical Methods in Engineering*, 74:1262 – 1277, 05 2008.
 - [3] Moritz Keuthen and D. Kraft. Shape optimization of a breakwater. *Inverse Problems in Science and Engineering*, 24, 09 2015.
 - [4] Bijan Mohammadi and Afaf Bouharguane. Optimal dynamics of soft shapes in shallow waters. *Computers & Fluids*, 40:291–298, 01 2011.
 - [5] Afaf Bouharguane and Bijan Mohammadi. Minimization principles for the evolution of a soft sea bed interacting with a shallow. *International Journal of Computational Fluid Dynamics*, 26:163–172, 03 2012.
 - [6] Adhémar-Jean-Claude Barré de Saint-Venant. Théorie du mouvement non-permanent des eaux, avec application aux crues des rivières et à l'introduction des marées dans leur lit. *C. R. Acad Sci Paris*, 08 1871.
 - [7] Kyung K. Choi. Shape design sensitivity analysis and optimal design of structural systems. In Carlos A. Mota Soares, editor, *Computer Aided Optimal Design: Structural and Mechanical Systems*, pages 439–492. Springer Berlin Heidelberg, 1987.
 - [8] Jan Sokołowski and Jean Paul Zolésio. *Introduction to Shape Optimization: Shape Sensitivity Analysis*. Springer series in computational mathematics. Springer-Verlag, 1992.
 - [9] Michel C. Delfour and Jean-Paul Zolésio. *Shapes and Geometries*. Society for Industrial and Applied Mathematics, second edition, 2011.
 - [10] Volker Schulz, Martin Siebenborn, and Kathrin Welker. Structured inverse modeling in parabolic diffusion processes. *SIAM Journal on Control and Optimization*, 53, 09 2014.
 - [11] Volker Schulz, Martin Siebenborn, and Kathrin Welker. Efficient pde constrained shape optimization based on steklov–poincaré-type metrics. *SIAM Journal on Optimization*, 26(4):2800–2819, 2016.
 - [12] Volker Schulz and Martin Siebenborn. Computational comparison of surface metrics for pde constrained shape optimization, 2016.
 - [13] Simon W. Funke, P.E. Farrell, and Matthew D. Piggott. Tidal turbine array optimisation using the adjoint approach. *Renewable Energy*, 63:658 – 673, 2014.
 - [14] Lino Alvarez-Vázquez, Aurea Martinez, Miguel Vázquez-Méndez, and M. Vilar. An optimal shape problem related to the realistic design of river fishways. *Ecological Engineering*, 06 2006.
 - [15] Mostafa Kadir. *Shape Optimization and Applications to Hydraulic Structures Mathematical Analysis and Numerical Approximation*. Doctoral thesis, 2019.
 - [16] Ven Te Chow. *Open-Channel Hydraulics*. The Blackburn Press, 1959.
 - [17] Per-Olof Persson and J. Peraire. Sub-cell shock capturing for discontinuous galerkin methods. *AIAA paper*, 2, 01 2006.
 - [18] Oksana Guba, Mark Taylor, Paul Ullrich, James Overfelt, and Michael Levy. The spectral element method on variable-resolution grids: Evaluating grid sensitivity and resolution-aware numerical viscosity. *Geoscientific Model Development Discussions*, 7, 06 2014.
 - [19] Joseph Oliger and Arne Sundström. Theoretical and practical aspects of some initial boundary value problems in fluid dynamics. *SIAM Journal on Applied Mathematics*, 35(3):419–446, 1978.
 - [20] Grégoire Allaire, François Jouve, and Georgios Michailidis. Thickness control in structural optimization via a level set method. *Structural and Multidisciplinary Optimization*, 53, 06 2016.
 - [21] Martin Berggren. A unified discrete-continuous sensitivity analysis method for shape optimization. In *CSC 2010*, 2010.
 - [22] Kathrin Welker. *Efficient PDE Constrained Shape Optimization in Shape Spaces*. doctoralthesis, Universität Trier, 2017.
 - [23] Martin S. Alnæs, Jan Blechta, Johan Hake, August Johansson, Benjamin Kehlet, Anders Logg, Chris Richardson, Johannes Ring, Marie E. Rognes, and Garth N. Wells. The fenics project version 1.5. *Archive of Numerical Software*, 3(100), 2015.
 - [24] Richard M. Beam, Robert F. Warming, and H. C. Yee. Stability analysis of numerical boundary conditions and implicit difference approximations for hyperbolic equations. *Journal of Computational Physics*, 48:200–222, 1982.

- [25] Vadym Aizinger and Clint Dawson. A discontinuous galerkin method for two-dimensional flow and transport in shallow water. *Advances in Water Resources*, 25(1):67 – 84, 2002.
- [26] Tuomas Kärnä, Benjamin de Brye, Olivier Gourgue, Jonathan Lambrechts, Richard Comblen, Vincent Legat, and Eric Deleersnijder. A fully implicit wetting–drying method for dg-fem shallow water models, with an application to the scheldt estuary. *Computer Methods in Applied Mechanics and Engineering*, 200(5):509 – 524, 2011.
- [27] Abdul Khan and Wencong Lai. *Modeling Shallow Water Flows Using the Discontinuous Galerkin Method*. 03 2014.
- [28] Ralf Hartmann. Numerical analysis of higher order discontinuous galerkin finite element methods, 10 2008.
- [29] Paul Houston and Nathan Sime. Automatic symbolic computation for discontinuous galerkin finite element methods, 2018.
- [30] Yulong Xing and Chi-Wang Shu. A new approach of high order well-balanced finite volume weno schemes and discontinuous galerkin methods for a class of hyperbolic systems with source. *Communications in Computational Physics*, 1, 02 2006.
- [31] Christophe Geuzaine and Jean-François Remacle. Gmsh: A 3-d finite element mesh generator with built-in pre- and post-processing facilities. *International Journal for Numerical Methods in Engineering*, 79:1309 – 1331, 09 2009.
- [32] Alexandros Avdis, Christian Jacobs, Simon Mouradian, Jon Hill, and Matthew Piggott. Meshing ocean domains for coastal engineering applications. In *VII European Congress on Computational Methods in Applied Sciences and Engineering*, 06 2016.
- [33] Marie Rognes, D. Ham, C. Cotter, and A. McRae. Automating the solution of pdes on the sphere and other manifolds in fenics 1.2. *Geoscientific Model Development*, 6, 12 2013.
- [34] Pierre-Antoine Absil, Robert Mahony, and Rodolphe Sepulchre. *Optimization Algorithms on Matrix Manifolds*, volume 78. Princeton University Press, 12 2008.
- [35] Rafael Correa and Alberto Seeger. Directional derivative of a minmax function. *Nonlinear Analysis-theory Methods & Applications*, 9:13–22, 01 1985.

A Derivation of Adjoint Equations

Proof. We need to rewrite the weak form (29) as

$$\begin{aligned}
a(H, \vec{Q}, p, \vec{R}) = & \int_0^T \int_{\Omega} -\frac{\partial p}{\partial t} H \, dx \, dt + \int_{\Omega} [H(x, T)p(x, T) - H_0 p(x, 0)] \, dx \\
& + \int_0^T \int_{\Omega} -\vec{Q} \cdot \nabla p \, dx \, dt + \int_0^T \int_{\Gamma} p \vec{Q} \cdot \vec{n} \, ds \, dt \\
& + \int_0^T \int_{\Omega} -(H + z) \nabla \cdot (\mu_v \nabla p) \, dx \, dt \\
& + \int_0^T \int_{\Gamma} [\mu_v (H + z) \nabla p \cdot \vec{n} - p \mu_v \nabla (H + z) \cdot \vec{n}] \, ds \, dt \\
& + \int_0^T \int_{\Omega} -\frac{\partial \vec{R}}{\partial t} \cdot \vec{Q} \, dx \, dt + \int_{\Omega} [\vec{Q}(x, T) \cdot \vec{R}(x, T) - \vec{Q}_0 \cdot \vec{R}(x, 0)] \, dx \\
& + \int_0^T \int_{\Omega} -\frac{\vec{Q}}{H} \cdot \nabla \vec{R} \cdot \vec{Q} \, dx \, dt + \int_0^T \int_{\Gamma} \frac{\vec{Q}}{H} \cdot \vec{R} \vec{Q} \cdot \vec{n} \, ds \, dt \\
& + \int_0^T \int_{\Omega} -\frac{1}{2} g H^2 \nabla \cdot \vec{R} \, dx \, dt + \int_0^T \int_{\Gamma} \frac{1}{2} g H^2 \vec{R} \cdot \vec{n} \, ds \, dt \\
& + \int_0^T \int_{\Omega} -\vec{Q} \cdot \nabla \cdot (G(\mu_f) \nabla \vec{R}) \, dx \, dt + \int_0^T \int_{\Omega} g H \nabla z \cdot \vec{R} \, dx \, dt \\
& + \int_0^T \int_{\Gamma} [G(\mu_f) \vec{Q} \cdot \nabla \vec{R} \cdot \vec{n} - \vec{R} \cdot G(\mu_f) \nabla \vec{Q} \cdot \vec{n}] \, ds \, dt.
\end{aligned}$$

Inserting Boundary Conditions leads to

$$\begin{aligned}
 a(H, \vec{Q}, p, \vec{R}) = & \int_0^T \int_{\Omega} -\frac{\partial p}{\partial t} H \, dx \, dt + \int_{\Omega} [H(x, T)p(x, T) - H_0 p(x, 0)] \, dx \\
 & - \int_0^T \int_{\Omega} \vec{Q} \cdot \nabla p \, dx \, dt + \int_0^T \int_{\Gamma_2} p \vec{Q} \cdot \vec{n} \, ds \, dt \\
 & - \int_0^T \int_{\Omega} \frac{1}{2} g H^2 \nabla \cdot \vec{R} \, dx \, dt - \int_0^T \int_{\Omega} (H + z) \nabla \cdot (\mu_v \nabla p) \, dx \, dt \\
 & + \int_0^T \int_{\Gamma_2} -p \mu_v \nabla (H_1 + z) \cdot \vec{n} \, ds \, dt \\
 & + \int_0^T \int_{\Gamma_1, \Gamma_3} \mu_v (H + z) \nabla p \cdot \vec{n} \, ds \, dt + \int_0^T \int_{\Gamma_2} \mu_v H_1 \nabla p \cdot \vec{n} \, ds \, dt \\
 & - \int_0^T \int_{\Omega} \frac{\partial \vec{R}}{\partial t} \cdot \vec{Q} \, dx \, dt + \int_{\Omega} [\vec{Q}(x, T) \cdot \vec{R}(x, T) - \vec{Q}_0 \cdot \vec{R}(x, 0)] \, dx \\
 & - \int_0^T \int_{\Omega} \frac{\vec{Q}}{H} \cdot \nabla \vec{R} \cdot \vec{Q} \, dx \, dt + \int_0^T \int_{\Gamma_2} \frac{\vec{Q}}{H_1} \cdot \vec{R} \vec{Q} \cdot \vec{n} \, ds \, dt \\
 & + \int_0^T \int_{\Gamma_1, \Gamma_3} \frac{1}{2} g H^2 \vec{R} \cdot \vec{n} \, ds \, dt + \int_0^T \int_{\Gamma_2} \frac{1}{2} g H_1^2 \vec{R} \cdot \vec{n} \, ds \, dt \\
 & - \int_0^T \int_{\Omega} \vec{Q} \cdot \nabla \cdot (G(\mu_f) \nabla \vec{R}) \, dx \, dt + \int_0^T \int_{\Gamma_1, \Gamma_2, \Gamma_3} G(\mu_f) \vec{Q} \nabla \vec{R} \cdot \vec{n} \, ds \, dt \\
 & + \int_0^T \int_{\Omega} g H \nabla z \cdot \vec{R} \, dx \, dt.
 \end{aligned}$$

Differentiating for the state variable H leads to

$$\begin{aligned}
 \frac{\partial a(H, \vec{Q}, p, \vec{R})}{\partial H} = & \int_0^T \int_{\Omega} -\frac{\partial p}{\partial t} \, dx \, dt + \int_{\Omega} p(x, T) \, dx \\
 & + \int_0^T \int_{\Omega} -\nabla \cdot (\mu_v \nabla p) \, dx \, dt + \int_0^T \int_{\Gamma_1, \Gamma_3} [\mu_v \nabla p \cdot \vec{n}] \, ds \, dt \\
 & + \int_0^T \int_{\Omega} \frac{\vec{Q}}{H^2} \cdot \nabla \vec{R} \cdot \vec{Q} \, dx \, dt \\
 & + \int_0^T \int_{\Omega} -g H \nabla \cdot \vec{R} \, dx \, dt + \int_0^T \int_{\Gamma_1, \Gamma_3} g H \vec{R} \cdot \vec{n} \, ds \, dt \\
 & + \int_0^T \int_{\Omega} g \nabla z \cdot \vec{R} \, dx \, dt
 \end{aligned}$$

and for \vec{Q} to

$$\begin{aligned}
 \frac{\partial a(H, \vec{Q}, p, \vec{R})}{\partial \vec{Q}} = & \int_0^T \int_{\Omega} -\frac{\partial \vec{R}}{\partial t} \, dx \, dt + \int_{\Omega} \vec{R}(x, T) \, dx \\
 & - \int_0^T \int_{\Omega} \nabla p \, dx \, dt + \int_0^T \int_{\Gamma_2} p \vec{n} \, ds \, dt \\
 & - \int_0^T \int_{\Omega} \frac{1}{H} (\nabla \vec{R})^T \vec{Q} - \frac{1}{H} (\vec{Q} \cdot \nabla) \vec{R} \vec{Q} \, dx \, dt \\
 & + \int_0^T \int_{\Gamma_2} \frac{1}{H_1} (\vec{Q} \cdot \vec{n}) \vec{R} \, ds \, dt + \int_0^T \int_{\Gamma_2} \frac{1}{H_1} (\vec{Q} \vec{R}) \cdot \vec{n} \, ds \, dt \\
 & + \int_0^T \int_{\Omega} -\nabla \cdot (G(\mu_f) \nabla \vec{R}) \, dx \, dt + \int_0^T \int_{\Gamma_1, \Gamma_2, \Gamma_3} G(\mu_f) \nabla \vec{R} \vec{n} \, ds \, dt.
 \end{aligned}$$

Now if $\frac{\partial a(H, \vec{Q}, p, \vec{R})}{\partial U} = -\frac{\partial J_{1,2}}{\partial U}$ then $\frac{\partial \mathcal{L}}{\partial U} = 0$ is fulfilled. From this we get the adjoint in strong form with boundary and terminal conditions (30)-(33). \square

B Derivation of Shape Derivative

Proof. We regard the Lagrangian (28). As in [10], the theorem of Correa and Seger [35] is applied on the right hand side of

$$J_{1,2}(\Omega) = \min_U \max_P \mathcal{L}(\Omega, U, P). \quad (61)$$

The assumptions of this theorem can be verified as in [9]. We now apply the rule (19) for differentiating domain integrals, alongside with boundary conditions

$$\begin{aligned} d\mathcal{L}(\Omega, U, P) &= \\ &= \lim_{\epsilon \rightarrow 0^+} \frac{\mathcal{L}(\Omega_\epsilon; U, P) - \mathcal{L}(\Omega; U, P)}{\epsilon} \\ &= \frac{d^+}{d\epsilon} \mathcal{L}(\Omega_\epsilon, U, P)|_{\epsilon=0} = \frac{d^+}{d\epsilon} \mathcal{L}(\Omega_\epsilon, H, \vec{Q}, p, \vec{R})|_{\epsilon=0} \\ &= \int_{\Omega} \left[\int_0^T -D_m \left(\frac{\partial p}{\partial t} H \right) dt + D_m (H(x, T)p(x, T) - H_0 p(x, 0)) \right. \\ &\quad - \int_0^T D_m \left(\frac{\partial \vec{R}}{\partial t} \cdot \vec{Q} \right) dt + D_m (\vec{Q}(x, T) \cdot \vec{R}(x, T) - \vec{Q}_0 \cdot \vec{R}(x, 0)) \\ &\quad + \int_0^T D_m (\nabla \cdot \vec{Q} p) dt + \int_0^T D_m (\mu_v \nabla (H + z) \cdot \nabla p) dt \\ &\quad + \int_0^T D_m \left(\nabla \cdot \left(\frac{\vec{Q}}{H} \otimes \vec{Q} \right) \cdot \vec{R} \right) dt + \int_0^T D_m \left(\frac{1}{2} g \nabla H^2 \cdot \vec{R} \right) dt \\ &\quad + \int_0^T D_m (G(\mu_f) \nabla \vec{Q} : \nabla \vec{R}) dt + \int_0^T D_m (g H \nabla z \cdot \vec{R}) dt \\ &\quad + \operatorname{div}(\vec{V}) \left(\int_0^T -\frac{\partial p}{\partial t} H dt + H(x, T)p(x, T) - H_0 p(x, 0) \right. \\ &\quad + \int_0^T -\frac{\partial \vec{R}}{\partial t} \cdot \vec{Q} dt + \vec{Q}(x, T) \cdot \vec{R}(x, T) - \vec{Q}_0 \cdot \vec{R}(x, 0) + \int_0^T \nabla \cdot \vec{Q} p dt \\ &\quad + \int_0^T \mu_v \nabla (H + z) \cdot \nabla p dt + \int_0^T \nabla \cdot \left(\frac{\vec{Q}}{H} \otimes \vec{Q} \right) \cdot \vec{R} dt \\ &\quad + \int_0^T \frac{1}{2} g \nabla H^2 \cdot \vec{R} dt + \int_0^T G(\mu_f) \nabla \vec{Q} : \nabla \vec{R} + \int_0^T g H \nabla z \cdot \vec{R} dt \Big] dx \\ &\quad + \int_{\Gamma_1} \left[\int_{\tilde{T}} D_m (\nu_1 E \sigma_\alpha (H - H_{\text{cr}})) dt + \int_0^T D_m \left(\frac{\nu_2}{2} \|\vec{Q}\|_2^2 \right) dt \right. \\ &\quad + \operatorname{div}_{\Gamma_1}(\vec{V}) \left(\int_{\tilde{T}} \nu_1 E \sigma_\alpha (H - H_{\text{cr}}) dt + \int_0^T \frac{\nu_2}{2} \|\vec{Q}\|_2^2 dt \right) \Big] ds \\ &\quad + \int_{\Gamma_2} \left[\int_0^T -D_m (\mu_v \nabla (H_1 + z) \cdot \vec{n} p) dt \right. \\ &\quad + \operatorname{div}_{\Gamma_2}(\vec{V}) \left(\int_0^T -\mu_v \nabla (H_1 + z) \cdot \vec{n} p dt \right) \Big] ds, \end{aligned}$$

where $\operatorname{div}_{\Gamma} \vec{V} = \operatorname{div} \vec{V} - \vec{n} \cdot (\nabla \vec{V}) \vec{n}$ is the tangential divergence of the vector field \vec{V} . Now the product rule (21) yields

$$\begin{aligned} &= \int_{\Omega} \left[\int_0^T -D_m \left(\frac{\partial p}{\partial t} \right) H - \frac{\partial p}{\partial t} \dot{H} dt \right. \\ &\quad + \dot{H}(x, T)p(x, T) + H(x, T)\dot{p}(x, T) - H_0 \dot{p}(x, 0) \\ &\quad + \int_0^T D_m \left(\frac{\partial \vec{R}}{\partial t} \right) \cdot \vec{Q} - \frac{\partial \vec{R}}{\partial t} \cdot \dot{\vec{Q}} dt + \dot{\vec{Q}}(x, T) \cdot \vec{R}(x, T) \end{aligned}$$

$$\begin{aligned}
& + \vec{Q}(x, T) \cdot \dot{\vec{R}}(x, T) - \vec{Q}_0 \cdot \dot{\vec{R}}(x, 0) + \int_0^T \dot{p} \cdot \nabla \cdot \vec{Q} + p D_m(\nabla \cdot \vec{Q}) \, dt \\
& + \int_0^T (\mu_v D_m(\nabla(H+z)) \cdot \nabla p + \mu_v \nabla(H+z) \cdot D_m(\nabla p)) \, dt \\
& - \int_0^T D_m \left(\nabla \cdot \left(\frac{\vec{Q}}{H} \otimes \vec{Q} \right) \right) \cdot \vec{R} \, dt + \int_0^T \nabla \cdot \left(\frac{\vec{Q}}{H} \otimes \vec{Q} \right) \cdot D_m(\vec{R}) \, dt \\
& + \int_0^T \left(\frac{1}{2} g D_m(\nabla H^2) \cdot \vec{R} + \frac{1}{2} g \nabla H^2 \cdot D_m(\vec{R}) \right) \, dt \\
& + \int_0^T \left(D_m(G(\mu_f) \nabla \vec{Q}) : \nabla \vec{R} + G(\mu_f) \nabla \vec{Q} : D_m(\nabla \vec{R}) \right) \, dt \\
& + \int_0^T g \dot{H} \nabla z \cdot \vec{R} \, dt + \int_0^T g H D_m(\nabla z) \cdot \vec{R} \, dt + \int_0^T g H \nabla z \cdot \dot{\vec{R}} \, dt \\
& + \operatorname{div}(\vec{V}) \left(\int_0^T -\frac{\partial p}{\partial t} H \, dt + H(x, T) p(x, T) - H_0 p(x, 0) \right. \\
& + \int_0^T -\frac{\partial \vec{R}}{\partial t} \cdot \vec{Q} \, dt + \vec{Q}(x, T) \cdot \vec{R}(x, T) - \vec{Q}_0 \cdot \vec{R}(x, 0) + \int_0^T p \nabla \cdot \vec{Q} \, dt \\
& + \int_0^T \mu_v \nabla(H+z) \cdot \nabla p \, dt + \int_0^T \nabla \cdot \left(\frac{\vec{Q}}{H} \otimes \vec{Q} \right) \cdot \vec{R} \, dt \\
& + \int_0^T \left. \left[\frac{1}{2} g \nabla H^2 \cdot \vec{R} \, dt + \int_0^T G(\mu_f) \nabla \vec{Q} : \nabla \vec{R} + \int_0^T g H \nabla z \cdot \vec{R} \, dt \right] \right] \, dx \\
& + \int_{\Gamma_1} \left[\int_{\tilde{T}} \nu_1 \left(\frac{1}{4} g \rho H \sigma_{\alpha, H_{\text{cr}}}(H) + E \sigma_{\alpha, H_{\text{cr}}}(H) (1 - \sigma_{\alpha, H_{\text{cr}}}(H)) \right) \dot{H} \, dt \right. \\
& + \int_0^T \nu_2 \vec{Q} \cdot \dot{\vec{Q}} \, dt \\
& + \operatorname{div}_{\Gamma_1}(\vec{V}) \left(\int_{\tilde{T}} \nu_1 E \sigma_{\alpha, H_{\text{cr}}}(H) \, dt + \int_0^T \frac{\nu_2}{2} \|\vec{Q}\|_2^2 \, dt \right) \Big] \, ds \\
& + \int_{\Gamma_2} \left[\int_0^T -\mu_v \nabla(H_1+z) \cdot \vec{n} \dot{p} \, dt + \operatorname{div}_{\Gamma_2}(\vec{V}) \left(\int_0^T -\mu_v \nabla(H_1+z) \cdot \vec{n} p \, dt \right) \right] \, ds.
\end{aligned}$$

The non-commuting of the material derivative (22), (23) and (24) such as integration by parts, regrouping and the fact that the sediment moves along with the deformation leads to

$$\begin{aligned}
& = \int_{\Gamma_1} \left[\int_{\tilde{T}} \left(\frac{1}{4} g \rho H \sigma_{\alpha, H_{\text{cr}}}(H) + E \sigma_{\alpha, H_{\text{cr}}}(H) (1 - \sigma_{\alpha, H_{\text{cr}}}(H)) \right) \dot{H} \, dt \right. \\
& + \int_0^T \nu_2 \vec{Q} \cdot \dot{\vec{Q}} \, dt \Big] \, ds \\
& + \int_{\Omega} \left[\int_0^T \left(-\frac{\partial p}{\partial t} + \frac{1}{H^2} (\vec{Q} \cdot \nabla) \vec{R} \cdot \vec{Q} - g H (\nabla \cdot \vec{R}) - \nabla \cdot (\mu_v \nabla p) + g \nabla z \cdot \vec{R} \right) \dot{H} \right. \\
& + \left(-\frac{\partial \vec{R}}{\partial t} - \nabla p - \frac{1}{H} (\vec{Q} \cdot \nabla) \vec{R} - \frac{1}{H} (\nabla \vec{R})^T \vec{Q} - (\nabla \cdot (G(\mu_f) \nabla \vec{R})) \right) \cdot \dot{\vec{Q}} \\
& + \left(\frac{\partial H}{\partial t} + \nabla \cdot (\vec{Q} - \mu_v \nabla(H+z)) \right) \dot{p} \\
& + \left(\frac{\partial \vec{Q}}{\partial t} + \nabla \cdot \left(\frac{\vec{Q}}{H} \otimes \vec{Q} + \frac{1}{2} g H^2 \mathbf{I}_2 - G(\mu_f) \nabla \vec{Q} \right) + g H \nabla z \right) \cdot \dot{\vec{R}} \, dt \Big] \, dx \\
& + \int_{\Omega} \int_0^T \left[-(\nabla \vec{V})^T : \nabla \vec{Q} p - (\nabla \vec{V})^T : \nabla \vec{Q} \frac{\vec{Q}}{H} \cdot \vec{R} - (\nabla \vec{V} \vec{Q} \cdot \nabla) \frac{\vec{Q}}{H} \cdot \vec{R} \right.
\end{aligned}$$

$$\begin{aligned}
 & -gH(\nabla \vec{V})^T \nabla H \cdot \vec{R} - \mu_v \nabla(H+z)^T (\nabla \vec{V} + \nabla \vec{V}^T) \nabla p \\
 & -G(\mu_f) \nabla \vec{Q} \nabla \vec{V} : \nabla \vec{R} - G(\mu_f) \nabla \vec{Q} \nabla \vec{V}^T : \nabla \vec{R} \\
 & -gH \nabla \vec{V}^T \nabla z \cdot \vec{R} + \operatorname{div}(\vec{V}) \left\{ \frac{\partial H}{\partial t} p + \nabla \cdot \vec{Q} p + \frac{\partial \vec{Q}}{\partial t} \cdot \vec{R} \right. \\
 & + (\vec{Q} \cdot \nabla) \frac{\vec{Q}}{H} \cdot \vec{R} + \nabla \cdot \vec{Q} \frac{\vec{Q}}{H} \cdot \vec{R} + \frac{1}{2} g \nabla H^2 \cdot \vec{R} + gH \nabla z \cdot \vec{R} \\
 & \left. + \mu_v \nabla(H+z) \cdot \nabla p + (G(\mu_f) \nabla \vec{Q}) : \nabla \vec{R} \right\} dx dt \\
 & + \int_{\Gamma_1} \operatorname{div}_{\Gamma_1}(\vec{V}) \left[\int_{\bar{T}} \nu_1 E \sigma_{\alpha, H_\alpha}(H) dt + \int_0^T \frac{\nu_2}{2} \|\vec{Q}\|_2^2 dt \right] ds \\
 & + \int_{\Gamma_2} \operatorname{div}_{\Gamma_2}(\vec{V}) \left[\int_0^T -\mu_v \nabla(H_1+z) \cdot \vec{n} p dt \right] ds.
 \end{aligned}$$

Since outer boundaries are not variable, in general the deformation field \vec{V} vanishes in small neighbourhoods around Γ_1, Γ_2 and the material derivative is zero, hence the boundary integrals vanish. In addition, evaluating the Lagrangian in its saddle point, the first integrals vanish such that we obtain the shape derivative in its final form. \square